RESEARCH PAPER

Investigating the rapid diagnosis of gliomas from serum samples using infrared spectroscopy and cytokine and angiogenesis factors

**James R. Hands · Peter Abel · Katherine Ashton ·
Timothy Dawson · Charles Davis · Robert W Lea ·
Alastair J S McIntosh · Matthew J Baker**

Abstract The ability to diagnose brain cancer rapidly from serum samples is of great interest; such a diagnosis would allow for rapid testing and time to results providing a responsive diagnostic environment, ability to monitor treatment efficacy, early detection of recurrent tumours and screening techniques. Current methods rely upon subjective, time-consuming tests such as histological grading and are particularly invasive with the diagnostic test requiring hospitalisation of 2–3 days. A rapid diagnostic method based upon serum samples would allow for a relatively non-invasive test and open up the possibility of screening for brain cancer. We report for the first time the use of a Bioplex immunoassay to provide cytokine and angiogenesis factor levels that differ between serum from glioma and non-cancer patients specifically angiopoietin, follistatin, HGF, IL-8, leptin, PDGF-BB and PECAM-1 providing sensitivities and specificities as high as 88 % and 81 %, respectively. We also report, for the first time, the use of serum ATR-FTIR combined with a RBF SVM for the diagnosis of gliomas from non-cancer patients with sensitivities and specificities as high as 87.5 % and 100 %, respectively. We describe the combination of these techniques in an orthogonal diagnostic regime, providing strength to the diagnosis through data combinations, in a rapid diagnostic test within 5 h from serum collection (10 min for ATR-FTIR and 4 h for the Bioplex Immunoassay). This regime has the ability to revolutionise the clinical environment by providing objective measures for diagnosis allowing for increased efficiency with corresponding decreases in mortality, morbidity and economic impact upon the health services.

Keywords Infrared · Orthogonal · Rapid · Glioma · Cytokines · Angiogenesis

J. R. Hands · A. J. S. McIntosh · M. J. Baker (✉)
Centre for Materials Science, Division of Chemistry, University of Central Lancashire, JB Firth Building, Preston PR1 2HE, UK
e-mail: mjbaker@uclan.ac.uk

P. Abel (✉) · R. W. Lea
School of Pharmacy and Biomedical Sciences, University of Central Lancashire, Maudland Building, Preston PR1 2HE, UK
e-mail: pabel@uclan.ac.uk

K. Ashton · T. Dawson · C. Davis
Department of Pathology, Lancashire Teaching Hospitals NHS Trust, Royal Preston Hospital, Sharoe Green Lane North, Preston, Lancashire PR2 9HT, UK

A. J. S. McIntosh
Department of Chemistry, Imperial College London, South Kensington Campus, London SW7 2AZ, UK

Introduction

Gliomas are the commonest primary tumours of the brain and comprise about 2 % of all newly diagnosed cancers every year in the UK. Overall, the incidence of gliomas roughly equals that of leukaemia [1]. Gliomas form about 50 % of all intracranial tumours in the adult, of which half are malignant gliomas. A glioma is composed of several heterogeneous malignant cell populations with a mixture of some normal cells [1]. Malignant gliomas comprise glioblastoma [World Health Organization (WHO) grade IV], anaplastic astrocytoma (WHO grade III), mixed anaplastic oligoastrocytoma (WHO grade III) and anaplastic oligodendroglioma (WHO grade III) [2]. The authors point the reader to the WHO classification of tumours of the central nervous system for further information on brain tumour classifications [3].

Early clinical diagnosis of glioma can be challenging; after a clinical suspicion the diagnosis is made by imaging with computed tomography (CT) and magnetic resonance imaging (MRI) scans, and by the time a patient presents with symptoms the diagnosis is fairly obvious on a CT scan [1]. Confirmation of diagnosis is done with the histological examination of the specimen obtained surgically; a biopsy of the brain involves

drilling through the skull to obtain a specimen that is hoped to be representative of the sample. At this point, there is no indication as to the whether the tumour is benign or malignant. It is clear now that tumours within a single histologically defined category are heterogeneous from a molecular genetic perspective. Histological grading is not able to provide accurate prognostic and therapeutic information for individual patients [1].

The primary requirement for successful treatment of any disease is early detection. Cancer incidence rates continue to rise [4]; however, survival rates for cancer are increased with early diagnosis. Early diagnosis of cancer such as prostate cancer (CaP) has increased the percentage of patients who survive more than 5 years after diagnosis [5]. Several cancers are in positions that are difficult to access, e.g. brain, which impacts negatively upon their detection. Research performed into identification of protein expression in blood has produced single biomarkers for specific cancers that have become misleading. The prostate-specific antigen (PSA) test is used to indicate CaP; however, approximately 40 % of organ-confined CaP show no elevation of PSA [6] and many other benign conditions can show increased PSA serum, thus producing false positives in screening. Hoffman et al. suggest that CaP screening would benefit from improved biomarkers, which more readily identify clinically important cancers [7]. As cancer is a heterogeneous disease, a set of markers or a whole sample profile will provide significantly more diagnostic information than any one marker [8]. Detecting disease rapidly has many benefits, including early intervention of therapy, reduction in mortality and morbidity, and freeing much needed economic resources within healthcare. Also, the identification of some indicator of disease could be used to monitor the progression of therapy [9]. The current 'gold standard' diagnostic method of histopathology takes between 24 and 72 h.

Cytokines and angiogenesis factors are being increasingly studied in order to understand their importance within cancer mechanisms. Cytokines and angiogenesis have been profiled in head and neck cancers [10], and their prognostic value has been investigated for pancreatic cancer [11]. Cytokines play an important role in modulating the immune responses to tumour growth and development. They can influence the growth and spread of tumours through the recruitment of pro-inflammatory cell types that can also affect angiogenesis. They can also act more directly by promoting or inhibiting tumour cell growth and have variable effects and influence on tumourigenesis and growth.

Angiogenesis is the proliferation of novel blood vessels from ones already formed and is a complex interaction of molecular signalling events that herald the process of basement membrane degradation, the proliferation of endothelial cells, the recruitment of perivascular cells and the invasion of the adjacent stromal space [12]. The process of angiogenesis is influenced by cytokines and growth factors as well as enzymes and adhesion molecules.

If a direct or indirect link from peripheral secretion to tumour cell expression and hence pathological progress could be demonstrated, then this would make analysis and monitoring of peripheral blood cytokine and angiogenic factors an ideal candidate for clinically useful biomarkers.

Vibrational spectroscopic techniques, such as Raman and FTIR, are excellent methods for the analysis of a wide range of materials. They are non-destructive, rapid, cost-effective, simple to operate and require only simple sample preparation. A relatively developed market in handheld instruments means they provide a unique capability for point-of-care diagnosis. Different biomolecules exhibit responses to different wavelengths of light; the resultant spectrum can be thought of as a 'fingerprint' of the sample. Spectroscopic analysis allows the objective classification of biological material on a molecular level. Previous studies have demonstrated the use of spectroscopy (imaging and point spectra) to analyse gastro-intestinal (GI) tract, lung, cervix, brain, breast, prostate and lymph node cancers [13–27].

Orthogonal diagnostic testing is the key to improving the reliability of rapid diagnostic technologies. Orthogonal testing refers to tests that are independent or non-overlapping but in combination provide a higher degree of accuracy of the final result [28]. Current single diagnostic modalities, specifically single biomarkers, are limited in their sensitivity and specificity; an orthogonal approach seeks to overcome these limitations with the strength of data combination [29]. We present, for the first time, the rapid diagnosis of WHO grade IV (glioblastoma multiforme) brain tumours based upon an orthogonal testing regime combining specific biochemical markers and spectroscopic signatures. The orthogonal approach provides strength to the result and has direct applicability within the clinical environment, allowing for increased efficiency within the diagnostic regime with corresponding decreases in mortality, morbidity and economic impact upon the health services.

Materials and methods

Serum samples

Blood samples were collected from 50 patients with clinically confirmed GBM brain tumours and 25 normal patients. Samples were obtained from the Walton Research Tissue Bank and Brain Tumour North West (BTNW) Tissue Bank; all patients had given research consent. Only newly diagnosed patients with a histopathological diagnosis of GBM (WHO grade IV) were included. All blood samples were taken pre-operatively. The serum tubes were left to clot at room temperature for a minimum of 30 min and a maximum of 2 h from blood draw to centrifugation. Separation of the clot was accomplished by centrifugation at 1,200×g for 10 min and

500-μl aliquots of serum dispensed into prelabelled cryovials. Serum samples were snap frozen using liquid nitrogen and stored at −80 °C. Demographic data for each patient was also stored on the tissue bank database and could be unblended by a member of the clinical team caring for the patient. The research described in this paper was performed with full ethical approval (BTNW and Walton Research Tissue Bank Application number 1108; applicant—P. Abel).

The average age of the entire sample set is 60.18 years. Average ages and age ranges for the GBM serum samples, and control serum samples are 60.22 (25–79) and 60.16 (26–87) years, respectively. Where possible, age and sex of the GBM and control serum samples were matched.

Bioplex suspension array

The Bioplex suspension array system was used to quantitate the cytokine and angiogenesis factor secretion. The technology incorporates 100 colour-coded bead sets each of which is conjugated to a specific reactant.

An antibody directed against a specific cytokine/angiogenesis factor is coupled to colour-coded beads. The antibody-coupled beads are allowed to react with the serum sample (for 30 min). After washing, a biotinylated antibody directed to a different epitope on the specific cytokine/angiogenesis factor is added to the beads. This forms a sandwich of antibodies around the cytokine. The reaction mixture is detected by the addition of streptavidin–phycoerythrin which binds to the biotinylated detection antibodies.

Identification is based around a laminar flow system of flow cytometry that identifies and quantitates each specific reaction based on bead colour and fluorescence. The magnitude of the reaction is measured using fluorescently labelled reporter molecules associated with each target protein. The quantities are expressed as picograms per milliliter based upon standard curves. Unknown concentrations are calculated from a standard curve generated from Bio-Rad supplied standards.

A verification and calibration procedure of the Bioplex analyser was carried out according to the manufacturer's instructions before analysis took place. Manufacturer-supplied reagents from different batches were used to confirm the accuracy, precision and reproducibility of the analytical technique used. Samples were performed in duplicate on a 96-well plate alongside the standard curve used to generate the results. Two wells with only manufacturer's diluents were used as blanks, and the resultant background reading levels were subtracted from all sample results.

Cytokine and angiogenesis factor data analysis

Initial data analysis was performed in the instrumentation software Bioplex manager version 4.1 following that the data

was exported to Microsoft Excel. *p*-values were calculated using the data analysis function on Microsoft Excel using a *t*-test assuming unequal variances. Confidence intervals were calculated by using the data analysis function on Microsoft Excel, and the sensitivity and specificity were determined by applying the confidence interval to the control mean to generate a reference range. The number of true and false positives and negatives among the patient group and the control group were then calculated.

Measures of sensitivity and specificity were used to assess the quality of discrimination. Sensitivity (Eq. 1) measures the ability of the model to correctly classify, whereas specificity (Eq. 2) measures its ability not to misdiagnose.

Equation for sensitivity

$$\text{Sensitivity} = \frac{True\ Positives}{True\ Positives + False\ Negatives} \quad (1)$$

Equation for specificity

$$\text{Specificity} = \frac{True\ Positives}{True\ Negatives + False\ Positives} \quad (2)$$

Definitions:

True Positives	Number of spectra where samples were correctly identified as cancerous
True Negatives	Number of spectra where the samples have been correctly identified as non-cancerous
False Positives	Number of spectra where the model has incorrectly identified the samples as cancerous when it is non-cancerous
False Negatives	Number of spectra where the model has incorrectly identified samples as non-cancerous when it is cancerous

Immunohistochemical tissue staining

Immunohistochemical staining of formalin-fixed, paraffin-embedded tissue sections of the patients used for the serum analysis was performed using antibodies raised against Follistatin-288 (provided by AbD Serotec, diluted 1:500). The secondary antibody, blocking reagents, avidin–biotin complex and chromagen were provided in kit form (PK6200 Elite—Universal Vectastain; Vector Labs). The slides were deparaffinised with xylene and rehydrated. Antigen retrieval was done in sodium citrate pH 6.0 using a pressure cooker in an 850-W microwave oven set for 2 min until the liquid was boiling. The manufacturer's protocol for staining was adhered to using Tris-buffered saline (pH 7.4) as the washing reagent. The incubation time for the blocking serum was 20 min and the incubation time for the primary and secondary antibody was 30 min. The coloured product was developed using horseradish peroxidase (HRP) as the enzyme and 3,3′-

diaminobenzidine (DAB) as the substrate. The slides were then counterstained with haematoxylin and washed with hot tap water. They were then dehydrated in alcohol and cleared with xylene and mounted in Pertex. Both tumour sample and non-cancerous brain sample were stained concurrently.

ATR–FTIR spectral collection

A JASCO FTIR-410 (Fourier transform infrared) Specac ATR single reflection diamond Golden Gate™ spectrometer was used in absorption mode to collect spectra from all serum samples at the University of Central Lancashire.

Prior to spectral collection, all whole serum samples were thawed and 10-kDa filtration aliquots were prepared using Amicon® Ultra 0.5-ml Millipore centrifugal filters. For each whole GBM serum and control serum sample, 0.5 ml of serum was inserted into the filtration devices and spun at 14,000 rpm for 15 min, resulting in two serum sample sets. Whole serum and serum with components above 10 kDa were filtered out.

Serum samples were analysed in a random order within the whole and 10-kDa serum sample sets. For each sample, the following procedure was repeated 3 times: 1 μl spot of serum was dried for 8 min on the ATR–FTIR crystal, at which time 3 spectra were collected. As a result, for each sample nine spectra were collected. A background absorption spectrum (taken for atmospheric correction) was taken prior to the serum being pipetted (a background per serum replicate) onto the crystal, and the dried serum film was washed off the crystal in between each procedure. Spectra were acquired at a resolution of 4 cm^{-1}, in the range of 4,000–400 cm^{-1} and averaged over 32 co-added scans. In total, 666 ATR–FTIR spectra were obtained from the 74 GBM and control serum samples. Forty nine GBM and 25 control serum samples were used for this study, one less than the Bioplex assay due to the amount available from that one sample.

ATR–FTIR data analysis

Initial analysis was performed using the JASCO Spectra Manager software. Spectra were organised into two sets, on a patient level:

Table 1 The optimal Cost and Gamma values for the whole serum and 10-kDa serum training data sets along with their corresponding cross-validation values

	Whole serum data	10 kDa serum data
Optimal Cost (C)	1,024	16,384
Optimal Gamma (γ)	8	16
Cross-validation	99.80 %	99.30 %

Table 2 The optimal Cost and Gamma values for the whole serum and 10-kDa serum training data sets along with their corresponding cross-validation values

Cytokine/ angiogenesis factor	Control mean (pg/ml)	GBM mean (pg/ml)	Significance ($P<0.05$)
IL-2	2.060	2.113	No
IL-4	0.204	0.225	No
IL-6	3.731	2.625	No
IL-10	3.113	5.477	No
GM-CSF	0.000	0.808	No
TNF-α	8.538	8.503	No
Angiopoietin	282.326	195.138	Yes
Follistatin	407.967	757.480	Yes
G-CSF	27.343	40.830	No
HGF	915.658	1,073.045	Yes
IL-8	20.133	16.374	Yes
Leptin	5,452.401	9,102.635	Yes
PDGF-BB	2,817.792	4,866.840	Yes
PECAM-1	2,734.137	3,832.264	Yes
VEGF	64.292	69.336	No

1. A training set containing 450 spectra (two thirds of the spectra)
2. A blind test set containing 216 spectra (one third of the spectra)

The fingerprint region (1,800–900 cm^{-1}) was selected for analysis and a visual spectral quality test, for gross spectral error, was implemented. A radial basis function kernel linear Support Vector Machine (SVM) model was used to simplify parameter optimisation and to allow for any non-linearity within the datasets. The LibSVM 3.12 [30] package was used and implemented via MATLAB®. A Support Vector Machine has previously been shown as a powerful tool for multivariate analysis of IR [31] and Raman spectra [32]. The optimal Cost and Gamma parameters values for the SVM kernel were obtained by a grid search combined with leave-one-out cross-validation. An initial wide parameter grid search was performed

Table 3 Sensitivity and specificity values for the statistically significant cytokine and angiogenesis factors

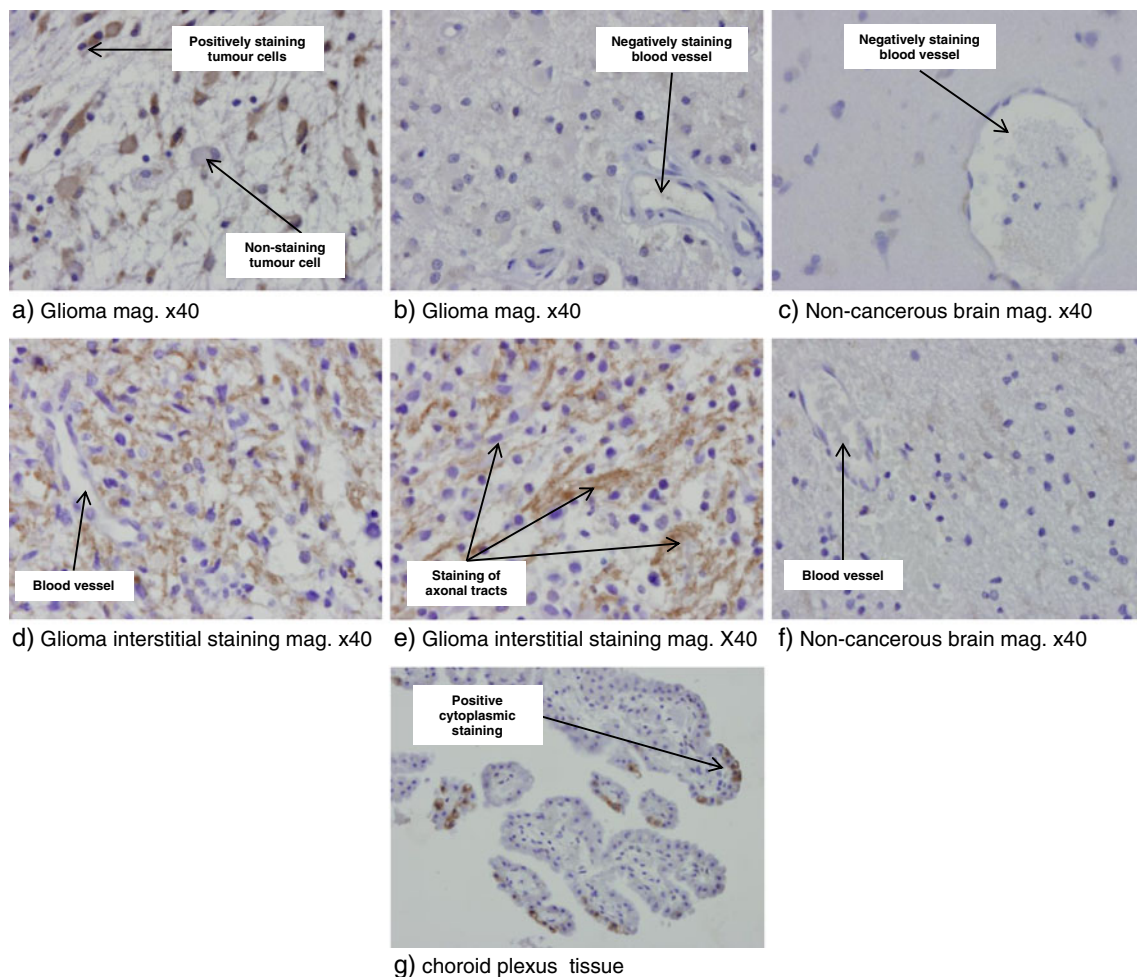| Cytokine/angiogenesis factor	Sensitivity (%)	Specificity (%)
Angiopoietin	58	63
Follistatin	88	81
HGF	46	74
IL-8	49	60
Leptin	40	74
PDGF-BB	82	66
PECAM-1	66	59

Fig. 1 Results of immunohistochemical staining for follistatin on glioblastoma multiforme and non-cancerous brain tissue

and the results used to perform a narrow grid search identifying the optimal parameter values. The SVM model was then trained using these values (Table 1) before being challenged with the bind test set.

Results and discussion

Cytokines and angiogenesis factors

Table 2 shows the levels of tested cytokine and angiogenesis factors for GBM and control samples along with the p-value for each analyte. The analytes that show a statistical difference between control serum and GBM are angiopoietin, follistatin, human growth factor, interleukin-8, leptin, platelet-derived growth factor-BB (PDGF-BB) and platelet endothelial cell adhesion molecule-1 (PECAM-1). The signalling pathways of angiogenesis in GBM are controlled mainly by the vascular endothelial growth factor (VEGF) family of molecules and receptors as well as others such as angiopoietin, platelet-derived growth factor (PDGF), interleukin-8 (IL-8), follistatin, hepatocyte growth factor (HGF), transforming growth factor beta (TGF-β), TGF-α and tumour necrosis factor alpha (TNF-α) [33–36]. Therefore, the identified analytes can be attributed to angiogenesis within GBM. Table 3 shows the sensitivity and specificity achieved for each of these statistically significant cytokine and angiogenesis factors based upon a 95 % confidence interval.

The highest sensitivity and specificity is achieved for follistatin with 88 and 81 %, respectively. Follistatin has previously been detected by Becker et al. in glioblastomas; immunohistochemical staining showed follistation in glial tumour cells, whereas in normal brain it was restricted to neurons [36]. Figure 1 shows follistatin immunohistochemical staining for tumour identification. Some gliomas exhibited significant follistatin immunostaining of tumour cells, and many appeared to express a gemistocytic morphology. However, staining was not uniform throughout the tumour sample, and some cells were patently immuno-negative (Fig. 1a). Positive immunostaining was entirely cytoplasmic with no membrane or

Fig. 2 ATR–FTIR spectra for dried whole serum and 10-kDa filtered serum. The variable CO_2 has been removed and the spectra are offset for ease of visualisation
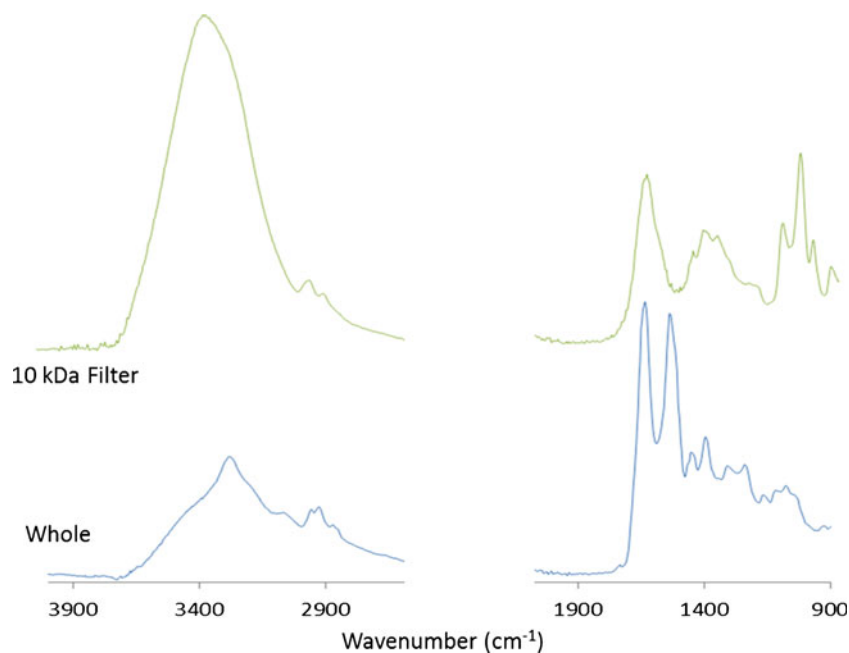
nuclear component, and other tissue elements within the sections, including blood vessels, were completely negative (Fig. 1b). There were no specific features of the tumours or constituent cells which were evidently predictive of immunopositivity or to account for the significant variability between individual tumours. The non-cancerous (viz. normal) brain tissue was uniformly negative throughout and there was no staining of either neurones or glial cells (Fig. 1c). There was a distinct interstitial stain in the presence of negatively staining cells that followed the axonal tracts of the sections (Fig. 1d, e). There was no specific axonal staining and some of the axonal tracts did not take up any stain. The non-cancerous brain axonal tracts were uniformly negative (Fig. 1f). There was some specific cytoplasmic staining of some cells from the choroid plexus (Fig. 1g). This may suggest that follistatin is being secreted into the cerebrospinal fluid (CSF) and warrants further detailed CSF analysis of angiogenesis-associated proteins. Follistatin is emerging as an interesting target in brain cancer research affecting migration and proliferation in glioblastoma, and may be a promising target for diagnosis and therapy [36].

ATR–FTIR diagnostic model

The primary concern for effective spectral collection via ATR–FTIR is intimate contact of the sample of interest with the ATR crystal as such the effect of drying of the serum sample upon the ATR–FTIR spectrum was investigated. Spectra taken at different times during the drying process show marked differences in spectral information with time as the serum dries and forms an intimate contact with the sample. Proposed biomolecular assignments for the dried whole serum ATR-FTIR spectrum (Fig. 2) are shown in Table 4. Repeat experiments

have shown that 1 μl of human serum is dry after 8 min at ambient room temperature (~18 °C) and pressure. The dried

Table 4 Proposed biomolecular assignments for spectral bands within the ATR–FTIR spectrum of a whole serum dried film (biomolecular assignments taken from refs. [38–48])

Wavenumber (cm^{-1})	Proposed biomolecular assignment
3,441	O–H stretch of hydroxyl groups
3,286	CH$_3$ stretch (antisymmetric), fatty acids, lipids, proteins
3,071	CH$_3$ stretch (antisymmetric), fatty acids, lipids, proteins
2,958	CH$_2$ stretch (antisymmetric), fatty acids, lipids, proteins
2,933	CH$_2$ stretch (antisymmetric), methylene group of membrane phospholipids
2866	CH$_2$ stretch (antisymmetric), fatty acids, lipids, proteins
1,741	C=O stretch (symmetric), fatty acids, lipids, proteins
1,637	Amide I of proteins (β-pleated sheet structures) ν C=O (80 %), ν C–N (10 %), δ N–H (10 %)
1,536	Amide II of proteins (β-pleated sheet structures) δ N–H (60 %), ν C–N (40 %)
1,449	CH$_2$ deformation of methylene group, lipids
1,399	CH$_3$ deformation, lipids
1,307	Lipids CH$_2$ twist, protein amide II band, cytosine, adenine
1,204	C–C stretch, C–H bend, PO$_2^-$ phosphodiester
1,170	C–O stretch (antisymmetric), COH bend, lipids
1,018	C–O stretch of glucose
924	C–C–N backbone, C–C stretch, glucose

Table 5 Patient-level results showing the number of misclassified spectra per patient based upon misclassified spectra from the blind test set challenge for the whole serum ATR–FTIR diagnostic model

Patient identifier	Misclassified spectra
GBM patients	
12012	1/9
12019	2/9
12055	5/9
11156	9/9
Non-cancer patients	
600	3/9
607	1/9

Table 7 Patient-level results showing the number of misclassified spectra per patient based upon misclassified spectra from the blind test set challenge for the 10-kDa filtered serum ATR–FTIR diagnostic model

Patient identifier	Misclassified spectra
GBM patients	
11121	6/9
11154	6/9
12019	6/9
12052	8/9
Non-cancer patients	
572	2/9
593	6/9
594	4/9

whole serum film shown is representative of the dried serum film described by Lie et al. [37]. The whole serum RBF SVM diagnostic model misclassified 21 out of 216 spectra when challenged with the blind test set resulting in a sensitivity of 88.2 % and specificity of 94.4 %. Table 5 shows the results of the blind test set challenge at a patient level for patients whose spectra were amongst the 21 misclassified. If more than four spectra from the nine taken for each patient group were classified as GBM or non-cancer, then this is regarded as the diagnosis. Only two patients with GBM were misclassified as non-cancer and zero non-cancer patients were diagnosed as GBM patients resulting in a sensitivity of 87.5 % and specificity of 100 % at the patient level.

The cytokine and angiogenesis factors identified as statistically significant via the Bioplex assay have a molecular weight range from 16 kDa to 32 kDa. In order to investigate if

Table 6 Proposed biomolecular assignments for spectral bands within the ATR–FTIR spectrum of a 10-kDa filtered serum dried film (biomolecular assignments taken from refs. [38–48])

Wavenumber (cm^{-1})	Proposed biomolecular assignment
3,308	O–H stretch of hydroxyl groups
2,941	CH$_3$ stretch (antisymmetric), fatty acids, lipids, proteins
2,883	CH$_2$ stretch (symmetric), methylene group of membrane phospholipids
1,641	Amide I of proteins (β-pleated sheet structures) ν C=O (80 %), ν C–N (10 %), δ N–H (10 %)
1,451	CH$_2$ deformation of methylene group, lipids
1,403	CH$_3$ deformation, lipids
1,345	Adenine, CH deformation
1,215	C–C stretch, C–H bend
1,107	PO$_2$ symmetric stretch
1,032	C–O RNA, ribose/glucose vibration
991	C–C stretch, C–N stretch, PO$_3$ stretch
916	C–C stretch, glucose

there are other biochemicals within the serum that are able to discriminate between GBM and non-cancer, the serum samples were filtered using a 10-kDa Amicon® Ultra 0.5-ml Millipore centrifugal filter, thus removing all moieties above 10 kDa from the serum samples. ATR–FTIR spectra for a dried whole serum sample and dried 10-kDa filtered sample are shown in Fig. 2 (offset for ease of visualisation), and proposed biomolecular assignments for the 10-kDa filtered spectrum are detailed in Table 6. The 10-kDa filtered RBF SVM diagnostic model misclassified 38 out of 216 spectra when challenged with the blind test set resulting in a specificity of 81.4 % and sensitivity of 81.9 %. Table 7 shows the results of the blind test set challenge at a patient level for patients whose spectra were amongst the 38 misclassified. Only four patients with GBM were misclassified as non-cancer and one non-cancer patient was diagnosed as a GBM patient resulting in a sensitivity of 78.9 % and specificity of 88.9 % at the patient level. The discriminatory power of the RBF SVM model is reduced compared to the whole serum model; however, the relatively high sensitivity and specificity indicate that there are biochemicals in the sub-10-kDa range that may provide interesting targets for diagnosis or prognosis.

Orthogonality

Using a two-stage diagnosis based upon follistatin levels and whole serum ATR–FTIR, a rapid orthogonal testing regime can be realised for brain cancer diagnosis (Table 8 shows the

Table 8 Patient-level results showing the misclassified patients based upon follistatin levels and whole serum ATR–FTIR diagnostic model

Test	False negatives	False positives
Follistatin level (95 % confidence interval)	11205, 11202	585, 594, 607, 609, 589
Whole serum ATR–FTIR	12055, 11159	

patients misclassified for each technique). ATR–FTIR can provide a result within 10 min of serum deposition (30 min for serum collection) and the Bioplex immunoassay within 4 h.

This orthogonal testing regime, built upon different phenomena (the concentration of cytokines and angiogenesis factor and the vibrational spectra of whole serum), allows for greater confidence in diagnosis due to the strength of data combination. Where both tests agree diagnosis is confirmed, where there are different results the serum sample is highlighted and the patient can be assessed via another diagnostic route such as immunohistochemistry, CT, MRI etc. The rapidity of the analysis allows for a dynamic and responsive clinical environment.

Conclusions

This work has shown, for the first time, the ability of specific biochemical markers and spectroscopic signatures to diagnose gliomas to sensitivities and specificities as high as 87.5 and 100 %, respectively. This new diagnostic regime is extremely rapid and when applied orthogonally can provide diagnosis within 5 h from serum collection. The technologies described are readily applicable to the clinical environment and have the potential to revolutionise diagnostic practices. The rapid information feedback allows for a dynamic and responsive clinical environment.

References

1. Iyer R. V, Golash A., Lea R W, Davies C, Roberts P (2006) Diagnosis and treatment of malignant glioma. Molecular and Cellular Pathology of Cancer Progression and Prognosis: Research Signpost 379–408
2. Stupp R, Tonn JC, Brada M, Pentheroudakis G (2010) High-grade malignant glioma: ESMO Clinical Practice Guidelines for diagnosis, treatment and follow-up. Ann Oncol 21(5):190–193
3. Loius DN, Ohgaki H, Wiestler OD, Cavenee WK, Burger PC, Jouvet A, Scheithauer W, Kleihues P (2007) The 2007 WHO Classification of Tumours of the Central Nervous System. Acta Neuropathol 114:97–109
4. XPrize Life Sciences Prize Group (2013) XPRIZE, CA, USA. http://www.xprize.org/prize-development/life-sciences. Accessed 3rd August 2012
5. Frankel S, Davey Smith G, Donovan J, Neal D (2003) Screening for prostate cancer. Lancet 361(9363):1122–1128
6. ERSPC Randomized Study of Screening for Prostate Cancer (2009) ERSPC, EU. http://media.erspc-media.org/erspc-background/#psa. Accessed 1st May 2012
7. Hoffman RM, Smith AY (2011) What we have learned from randomized trials of prostate cancer screening. Asian J Androl 13:369–373
8. Hessels D, Rittenhouse HG, Schalken JA (2005) Molecular diagnostics in prostate cancer. EAU Update Series 3(4):200–213
9. Ellis DI, Goodacre R (2006) Metabolic fingerprinting in disease diagnosis: biomedical applications of infrared and Raman spectroscopy. Analyst 131(8):875–885
10. Byers LA, Kies MS, William WN, Hu J, Lee JJ, El-Naggar A, Papadimitrakopoulou V, Myers JN, Lippman SM, Heymach JV (2008) Profiling of cytokines and angiogenic factors (C/AF) in head and neck (HN) cancer correlates circulating biomarkers with clinical outcomes following induction chemotherapy. Journal of Clinical Oncology, ASCO Annual Meeting Proceedings 26 (#6005)
11. Rahbari NN, Schmidt T, Falk CS, Hinz U, Herber M, Bork U, Büchler MW, Weitz J, Koch M (2011) Expression and prognostic value of circulating angiogenic cytokines in pancreatic cancer. BMC Cancer 11(286)
12. Jansen M, Hamer PCD, Witmer AN, Troost D, van Noorden CJF (2004) Current perspectives on antiangiogenesis strategies in the treatment of malignant gliomas. Brain Res Brain Res Rev 45(3):143–163
13. DaCosta RS, Wilson BC, Macron NC (2005) Optical techniques for the endoscopic detection of dysplastic colonic lesions. Curr Opin Gastroenterol 21:70–79
14. Shim M, Wong Kee Son LM, Marcon NE, Wilson BC (2000) *In vivo* near-infrared Raman spectroscopy: demonstration of feasibility during clinical gastrointestinal endoscopy. J Photochem Photobiol 72:146–150
15. Bakker Schutt TC, Puppels GJ, Kraan YM, Greve J, van der Maas LLJ (1997) Intracellular carotenoid levels measure by Raman microspectroscopy: comparison of lymphocytes form lung cancer patients and healthy individuals. Int J Cancer 74(1):20–25
16. Sulé-Suso J, Forster A, Zholobenko V, Stone N, El Haj A (2004) Effect of $CaCl_2$ and $MgCl_2$ on Fourier transform infrared spectra of lung cancer cells. Appl Spectrosc 58:61–67
17. Lyng FM, Faoláin EO, Conroy J, Meade AD, Knief P, Duffy B, Hunter MB, Byrne JM, Kelehan P, Byrne HJ (2007) Vibrational spectroscopy for cervical cancer pathology, from biochemical analysis to diagnostic tool. Exp Mol Pathol 82(2):121–129
18. Podshyvaloy A, Sahv RK, Mark S, Kantarovich K, Guterman H, Goldstein J, Jagannathan R, Argov S, Mordechai S (2005) Distinction of cervical cancer biopsies by use of infrared microspectroscopy and probabilistic neural networks. Applied Optics 44(1–2):3725–3734
19. Koljenović S, Choo-Smith LP, Schut TC, Kros JM, Berge HJ, Puppels GJ (2002) Discriminating vital tumour from necrotic tissue in human glioblastoma tissue by Raman spectroscopy. Lab Invest 82(10):1265–1277
20. Beleites C, Steiner G, Sowa MG, Baumgartner R, Sobottka S, Schackert G, Salzer R (2005) Classification of human gliomas by infrared imaging spectroscopy and chemometric image processing. Vibrational Spectroscopy 38:143–149
21. Manoharan R, Shafer KE, Perelman LT, Wu J, Chen K, Deinum G, Fitzmaurice M, Myles J, Crowe J, Dasari RR, Feld MS (1998) Raman spectroscopy and fluorescence photon migration for breast cancer diagnosis and imaging. Photochemistry and Photobiology 67(1):15–22
22. Dukor RK, Liebman MN, Johnson BL (1998) A new, non-destructive method for analysis of clinical samples with FT-IR microspectroscopy. Breast cancer tissue as an example. Cell Molecular Biology 44(1):211–217

23. Baker MJ, Gazi E, Brown MD, Shanks JH, Clarke NW, Gardner P (2009) Investigating FTIR based histopathology for the diagnosis of prostate cancer. Journal of Biophotonics 2(1–2):104–113

24. Malins DC, Polissar NL, Gunselman SJ (1997) Models of DNA structure achieve almost perfect discrimination between normal prostate, benign prostatic hyperplasia (BPH), and adenocarcinoma and have a high potential for predicting BPH and prostate cancer. Proceedings of the National Academy of Sciences of the United States of America 94(1):259–264

25. Fernandez DC, Rohit B, Hewitt SM, Levin IW (2005) Infrared spectroscopic imaging for histopathologic recognition. Nature Biotechnology 23:469–474

26. Isabelle M, Stone N, Barr H, Vipond M, Sheperd N, Rogers K (2008) Lymph node pathology using optical spectroscopy in cancer diagnostics. Spectroscopy 22:97–104

27. Romeo MJ, Diem M (2005) Infrared spectral imaging of lymph nodes: strategies for analysis and artefact reduction. Vibrational Spectroscopy 38(1–2):115–119

28. Wolcott M J, Schoepp R J, Norwood D A, Shoemaker D R (2007) Rapid infectious disease diagnostic assays, global infectious disease surveillance and detection: assessing the challenges—Find Solutions Workshop Summary 165–177

29. Henchel EA, Teska JD, Ludwig GV, Shoemaker DR, Ezzell JW (2001) Current laboratory methods for biological threat agent identification. Clin Lab Med 21(3):661–678

30. Chang C C, Lin C J (2011) LIBSVM: a library for support vector machines. ACM TIST 2.Doi:10.1145/1961189.1961199

31. Baker MJ, Clarke CC, Nicholson JM, Lyng FM, Byrne HJ, Hart CA, Brown MD, Clarke NW, Gardner P (2010) An investigation of the RWPE prostate derived family of cell lines using FTIR spectroscopy. Analyst 135(5):887–894

32. Sattlecker M, Bessant C, Smith J, Stone N (2010) Investigation of support vector machines and Raman spectroscopy for lymph node diagnostics. Analyst 135(5):895–901

33. Bouloumie A, Schini-Kerth VB, Busse R (1999) Vascular endothelial growth factor up-regulates nitric oxide synthase expression in endothelial cells. Cardiovascular Research 41(3):773–780

34. Reiss Y, Machein MR, Plate KH (2005) The role of angiopoietins during angiogenesis in gliomas. Brain Pathology 15(4):311–317

35. Dunn IF, Heese O, Black PM (2000) Growth factors in glioma angiogenesis: FGFs, PDGF, EGF, and TGFs. Journal of Neuro-Oncology 50(1–2):121–137

36. Becker M, Mertsch S, Schuch R, Paulus W, Senner V (2010) Follistatin promotes migration and proliferation of glioma cells. European Journal of Cell Biology 89:17–17

37. Liu KZ, Shaw AR, Man A, Dembinski TC, Mantsch HH (2002) Reagent-free, simultaneous determination of serum cholesterol in HDL and LDL by infrared spectroscopy. Clinical Chemistry 48(3):400–506

38. Baker MJ, Gazi E, Brown MD, Shanks JH, Gardner P, Clarke NW (2008) FTIR-based spectroscopic analysis in the identification of clinically aggressive prostate cancer. British Journal of Cancer 99:1859–1866

39. Diessel E, Willman S, Kamphaus P, Kurte R, Damm U, Heise HM (2004) Glucose quantification in dried-down nanolitre samples using mid-infrared attenuate total reflection spectroscopy. Applied Spectroscopy 58(4):442–450

40. Shaw RA, Mantsch HH (2010) Infrared spectroscopy in clinical and diagnostic analysis. Encyclopaedia of Analytical Chemistry. Wiley, Chichester

41. Goormaghtigh E, Raussens V, Ruysschaert JM (1999) Attenuated total reflection infrared spectroscopy of proteins and lipids in biological membranes. Biochimica et Biophysica Acta 1422:105–185

42. Rohleder D, Kocherscheidt G, Gerber K, Kiefer W, Kohler W, Mock J, Petrich W (2005) Comparison of mid-infrared and Raman spectroscopy in the quantitative analysis of serum. Journal of Biomedical Optics 10(3):031108

43. Naumann D (2001) FT-infrared and FT-Raman spectroscopy in biomedical research. Applied Spectroscopy Reviews 36(2–3):239–298

44. Meade A, Lyng F, Knief P, Byrne H (2007) Growth substrate induced functional changes elucidated by FTIR and Raman spectroscopy in in-vitro cultured human keratinocytes. Analytical and Bioanalytical Chemistry 387(5):1717–1728

45. Bellisola G, Sorio C (2012) Infrared spectroscopy and microscopy in cancer research and diagnosis. American Journal of Cancer Research 2(1):1–21

46. Tamm LK, Tatulian SA (1997) Infrared spectroscopy of proteins and peptides in lipid bilayers. Quarterly Reviews of Biophysics 30(4):365–429

47. Petrich W, Lewandrowski KB, Muhlestein JB, Hammond ME, Januzzi JL, Lewandrowski EL, Pearson RR, Dolenko B, Fruh J, Haass M, Hirschl MM, Kohler W, Mischler R, Mocks J, Ordonez-Llanos J, Quarder O, Somorjai R, Staib A, Sylven C, Werner G, Zerback R (2009) Potential of mid-infrared spectroscopy to aid the triage of patients with acute chest pain. Analyst 134(6):1092–1098

48. Gajjar K, Trevisan J, Owens G, Keating P, Wood N, Stringfellow H, Martin-Hirsch P, Martin F (2013) Fourier-transform infrared spectroscopy coupled with a classification machine for the analysis of blood plasma or serum: a novel diagnostic approach for ovarian cancer. Analyst. doi:10.1039/c3an36654e